

CO and O overlayers on Pd nanocrystals supported on TiO₂(110)

Chi Ming Yim,^a Chi Lun Pang,^a David S. Humphrey,^a
Christopher A. Muryn,^b Karina Schulte,^c Rubén Pérez^{de}
and Geoff Thornton^{*a}

Received 30th November 2012, Accepted 17th December 2012

DOI: 10.1039/c2fd20137b

We have prepared a model catalytic system by depositing Pd onto a TiO₂(110) surface held at ~720 K. Scanning tunneling microscopy (STM) reveals well-defined Pd nanocrystals consisting of (111) top facets with {111} and {100} side facets. The Pd nanocrystals go down to about 10 nm in width and 1.3 nm in height. Top facets can be imaged with atomic resolution, indicating the absence of TiO_x encapsulation. The model catalyst was probed by exposure to CO and O₂. By varying the CO exposure, different CO overlayers were formed on the (111) top facets, with coverages ranging from 0.33 to 0.75 of a monolayer. Near edge X-ray absorption fine structure (NEXAFS) measurements at 300 K reveal that at around 0.5 ML coverage, CO is oriented with the molecular axis more or less normal to TiO₂(110). Dosing small amounts of O₂ separately on a Pd/TiO₂(110) surface led to an overlayer of *p*(2 × 2)-O formed on the (111) top facet of the Pd nanocrystals at 190 K.

1 Introduction

The study of metal nanoparticles on oxide supports has received considerable attention, for reasons both practical and fundamental. On the practical side, the heterogeneous catalysts used in industrial applications usually consist of nanometer-sized metal particles distributed on an oxide support. In order to improve their performance, a better understanding of their properties is necessary. One method of achieving this is to investigate appropriate model catalyst systems. On the fundamental side, nanometer-sized metal particles have been shown to exhibit properties deviating from their corresponding single crystal surfaces. These differences have been shown to relate to the unique phenomena occurring in those systems such as kinetic interplay between facets,¹ spillover and reverse spillover of adsorbates between metal particles and their supports,² and the strong metal–support interactions (SMSI).³

Scanning probe methods such as STM and non-contact atomic force microscopy (NC-AFM) have been employed extensively over the past decade to investigate metal nanoparticles on metal oxide surfaces.^{1,4–8} Issues such as initial metal

^aDepartment of Chemistry and London Centre for Nanotechnology, University College London, 17–19 Gordon Street, London, WC1H 0AH, UK. E-mail: g.thornton@ucl.ac.uk

^bSchool of Chemistry & Photon Science Institute, The University of Manchester, Oxford Road, Manchester, M13 9PL, UK

^cThe MAX-IV Laboratory, Lund University, P.O. Box 118, 221 00 Lund, Sweden

^dLawrence Berkeley National Laboratory, 1 Cyclotron Road, Mail Stop 66-200, Berkeley, California, CA 94720, USA

^eUniversidad Autonoma de Madrid, Departamento de Fisica Teorica de la Materia Condensada, Facultad de Ciencias, Modulo C-5, E-28049 Madrid, Spain

adsorption site, spillover, and thermal stability have been studied. Despite this interest, only one of these studies has addressed the adsorption of gas molecules on supported nanoparticles. Højrup Hansen *et al.*⁸ studied NO and O₂ adsorption on Pd nanoparticles on an ultrathin alumina film, itself supported on NiAl(110). However, because their images were taken under a partial pressure of NO and O₂, their observations were limited to saturation coverages of these adsorbates. Under-saturated overlayers are important as further reaction is much more likely.

Here, we address the issue of gas adsorption on supported metal nanoparticles by studying the coverage-dependent adsorption of CO on Pd nanocrystals supported on TiO₂(110). Pd/TiO₂ systems attract much attention in surface science due to their use in a wide range of processes including nitrite reduction in drinking water,⁹ acetylene hydrogenation¹⁰ and automobile catalysis where interaction with CO is an important consideration.¹¹ Preparing chemically active, well-defined Pd nanoparticles on rutile TiO₂(110) is a difficult task that is hindered by the propensity for the Pd particles to become encapsulated with a TiO_x layer ($x < 2$) after annealing. The onset temperature for encapsulation is about 800 K.⁴ In addition to degrading the chemical reactivity (such as CO uptake),^{4,5} encapsulation also drastically alters the structure of the Pd islands.⁷ Similar encapsulation-induced structural changes were also discovered for Pt/TiO₂(110).⁶

STM experiments reveal the presence of well-ordered CO overlayers on top of the Pd nanoparticles. These overlayers have different structures depending on the CO coverage. Similar overlayers formed on the Pd(111) surface have also been observed using low energy electron diffraction (LEED),¹² X-ray photoelectron spectroscopy (XPS)/electron energy loss spectroscopy (EELS)¹³ and STM¹⁴ in the past, with their stability studied by Loffreda *et al.*¹⁵ using DFT theory. Here, we analyse the stability of the CO overlayers formed on the Pd nanoparticles using an exchange-correlation functional that includes van der Waals (vdW) non-local correlations. The vdW functional proposed by Dion *et al.*^{16,17} has been applied to the chemisorption of CO on the (111) surfaces of late 4d and 5d transition metals.¹⁸ This functional reduces or completely solves the well-known discrepancy between theory and experiment regarding CO site preference and improves the value of the adsorption energies. In our study, we have used the optimised vdW functional optB86b, recently introduced by Klimeš *et al.*,^{19,20} that improves significantly the accuracy of the original vdW-DF and reaches better than chemical accuracy for the S22 data set.²⁰

2 Experimental and theoretical methods

Synchrotron radiation spectroscopies at MAX-Lab

To investigate the bonding geometry of CO on the TiO₂(110)-supported Pd nanoparticles, we performed near-edge X-ray absorption fine structure (NEXAFS) measurements at Beamline I311 at MAX-lab. The beamline is described elsewhere.²¹ The analysis chamber is equipped with a SCIENTA-SES200 hemispherical analyzer for photoemission (XPS) and NEXAFS in Auger yield mode. The angle between the analyzer and the incident photon beam is 55°.

The TiO₂(110) sample was cleaned by cycles of Ar⁺ sputtering and annealing to ~1000 K. The sample temperature was checked using a K-type thermocouple spot-welded near the edge of the sample, which was mounted on a tantalum (Ta) sample holder. The sample cleanliness and long-range order were verified with XPS and LEED, respectively. Pd nanoparticles were formed by depositing Pd onto TiO₂(110) with the sample held at 800 K. Pd was evaporated from an *Omicron EFM3* electron-beam evaporator. Pd 3d and Ti 2p photoemission spectra ($h\nu = 620$ eV) were recorded to confirm the presence and chemical nature of Pd nanoparticles and to verify that no encapsulation had taken place on the Pd nanoparticles. All XPS were taken at normal emission. Binding energies were measured with respect to the Fermi edge (E_F) determined from the Ta sample plate in direct electrical

contact with the sample. Research-grade CO was dosed by backfilling the preparation chamber, with its purity verified with a quadrupole mass spectrometer.

Carbon K-edge NEXAFS ($h\nu = 280\text{--}320$ eV) measurements were carried out to examine the bonding geometry of CO on the Pd/TiO₂(110) surface. The degree of polarisation in the C K-edge region was estimated to be 0.94. NEXAFS data were recorded with the angle of incidence ranging between 40 and 90 degrees by monitoring the carbon KLL Auger yield. All NEXAFS and XPS measurements were carried out at 300 K.

STM experiments

The STM experiments were carried out with an *Omicron GmbH* low temperature STM housed in a bath cryostat within an ultrahigh vacuum (UHV) chamber (base pressure = 2×10^{-11} mbar). The adjoining preparation chamber was equipped with facilities for electron beam heating, ion sputtering, Pd deposition, XPS, LEED, and quadrupole mass spectroscopy (QMS).

The TiO₂(110)-(1 × 1) samples (*Pi-Kem*) were prepared through cycles of argon-ion sputtering (1 kV, drain current ~ 7 μ A) and annealing to 950 K. Sample cleanliness and long-range order were verified with XPS and LEED. Pd islands were formed by physical vapor deposition (PVD) onto the as-prepared TiO₂(110) surface with the sample held at 700–800 K. The Pd source consisted of Pd wire (*Advent*, 99.95%) wrapped around a tungsten filament that was resistively heated. CO (*Labor-gase*, 99.998%) was dosed mainly with a directional doser placed ~ 50 mm away from the STM stage or *via* backfilling with a leak valve in the preparation chamber. In one case, CO was first dosed from the residual vacuum. The directional doser consisted of a 0.25 inch stainless steel tube welded to a leak-valve. O₂ (*SIP Analytical Ltd.*, 99.999%) was dosed using the directional doser. The purity of both CO and O₂ were checked using QMS.

STM measurements were carried out with electrochemically etched tungsten tips (*Advent*, purity = 99.95 %, diameter = 0.25 mm). The tips were conditioned by vacuum annealing at 200 °C and voltage pulses during scanning. STM images were acquired at 124–190 K.

Computational details

The DFT calculations for the CO overlayers on a Pd(111) surface have been performed using the Vienna *ab initio* simulation package (VASP, version 5.2.12) with the projector-augmented wave (PAW) method and a cutoff of 500 eV for the plane-wave expansion of the wavefunctions.^{22,23} For the exchange-correlation functional, we have used the optB86b vdW functional implemented in VASP by Klimes *et al.*²⁰ using the algorithm of Román-Pérez and Soler.²⁴ A spin-restricted approach has been used since spin polarisation effects have been found to be negligible.

Geometry optimisations were performed on a supercell structure using periodic boundary conditions. The (111) surface is modeled by a four layer slab, with a CO adlayer on one side of the slab and a vacuum space equivalent to six ideal bulk metallic layers. We use the lattice constant of 3.946 Å calculated theoretically for Pd, that is close to the experimental value (3.82 Å). We have considered three different surface unit cells to simulate the different coverages: ($\sqrt{3} \times \sqrt{3}$)R30°-1CO (0.33 ML), $c(4 \times 2)$ -2CO (0.5 ML), and (2×2) -3CO (0.75 ML). The two uppermost substrate layers and the CO molecules are allowed to relax, while the bottom two layers of Pd atoms were held fixed in their bulk positions. All atomic coordinates of the adsorbed species and the metal atoms in the relaxed metal layers were optimised to a force of less than 0.01 eV Å⁻¹ on each atom. Brillouin zone integration was performed using Monkhorst–Pack grids of $12 \times 12 \times 1$, $8 \times 8 \times 1$ and $4 \times 4 \times 1$, for the ($\sqrt{3} \times \sqrt{3}$), (2×2) , and $c(4 \times 2)$ unit cells, respectively, and a Methfessel–Paxton smearing of 0.2 eV.

3 Results and discussion

NEXAFS measurements of CO on Pd/TiO₂(110)

A Pd/TiO₂(110) surface was prepared by depositing Pd onto the TiO₂(110) surface with the sample held at 800 K. This resulted in well-ordered Pd nanoparticles distributed on the TiO₂(110) surface, with their (111) top facets oriented parallel to the TiO₂(110) surface, as evidenced by the emergence of Pd(111)-(1 × 1) spots in LEED.²⁵ Ti 2p XPS peaks taken before and after the Pd dose showed no significant increase in the amount of Ti³⁺ and Ti²⁺ species, indicating that no encapsulation takes place on the Pd nanoparticles. Using the change in integrated intensity of Ti 2p_{3/2} peaks, the effective thickness of Pd present on the TiO₂(110) surface was calculated to be 10.4 ± 3.7 Å. Note that this value will depend on the morphology as well as the size distribution of the nanoparticles and is therefore only a nominal value.

After growing Pd nanoparticles on the TiO₂(110) surface, NEXAFS spectra of TiO₂(110)/Pd/CO were recorded in the photon energy range 280–320 eV at different angles of incidence from the Pd/TiO₂(110) surface before and after exposure of 2000 L CO (1 L = 1 langmuir = 1.33 × 10⁻⁶ mbar s) at 300 K. The kinetic energy window of the analyzer was centred at 265 eV with a width of 4.4 eV. To remove unwanted signals from the substrate, we normalised the NEXAFS spectra by subtracting the spectra before CO exposure from those recorded on the CO-covered surface. The resulting difference spectra are displayed in Fig. 1a.

Each spectrum in Fig. 1a consists of a peak at ~287.2 eV convoluted with a step-like feature. The peak corresponds to the π* resonance, in which the 1s electrons in carbon atoms are photo-excited to the unoccupied π* orbitals of CO. STM data (not shown) indicate that nearly 90% of the TiO₂(110) substrate is covered with Pd islands. Moreover, no CO adsorption on the TiO₂(110) surface was observed at 300 K. On this basis, we conclude that only CO bonded to the Pd islands contributes to the X-ray absorption signal. To determine the orientation of CO molecules on the Pd islands, taking threefold symmetry of the Pd islands into account, we numerically fitted the area of the π* resonance peak as a function of incident angle using the appropriate equations in ref. 26. The best fit to the data in Fig. 1b corresponds to

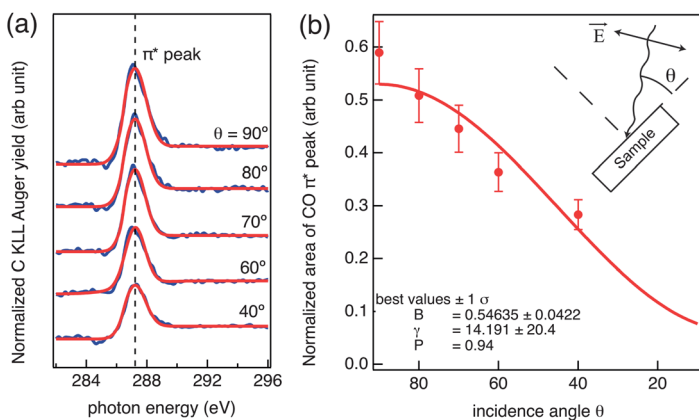


Fig. 1 (a) Normalised carbon KLL NEXAFS as a function of photon energy measured at different incident angles on CO-covered Pd nanoparticles grown on TiO₂(110), recorded at room temperature. Only the region of the π* resonant peak is shown. Blue dots are experimental data and red solid lines are numerical fits. (b) Normalised area of the CO π* resonant peak as a function of incident angle. Dots are experimental data, and the solid line is a numerical fit to the experimental data using the appropriate equations in Stöhr and Outka's paper ref. 26. The best-fit values shown are the arbitrary constant *B*, degree of polarisation *P* (= 0.94), and the angle between the C–O axis and the surface normal *γ*.

a bond angle, γ , of $14.2 \pm 22.1^\circ$. Hence, CO bonds more or less vertically on the top facet of the Pd islands.

CO overlayers at different coverages in STM

Pd was deposited on the rutile $\text{TiO}_2(110)$ substrate with the sample held at a temperature of ~ 720 K. This led to the formation of Pd nanoparticles distributed on the $\text{TiO}_2(110)$ surface, as shown in Fig. 2a. The shape of the particles is indicative of well-ordered nanocrystals comprised of a (111) top facet with {111} and {100} side facets. Their average heights and diameters are 2.38 ± 0.44 nm and 22.0 ± 5.2 nm, respectively. Occasionally, the top facet can be imaged with atomic resolution, as shown in Fig. 2b. The nearest-neighbour separation of bright protrusions is about 270 ± 10 pm, consistent with the Pd lattice constant, 275 pm, thus validating the suggestion that the top facet is a Pd(111)-(1 \times 1) face. It also demonstrates that the Pd nanocrystals formed in this way are not encapsulated.⁷ Note that due to the spatial limit of STM, we could not detect any lattice contraction of the (111) top facet as suggested in the micro-calorimetric measurements of CO on $\text{Fe}_3\text{O}_4(111)$ film-supported Pd nanoparticles by Fischer–Wolfarth *et al.*²⁷

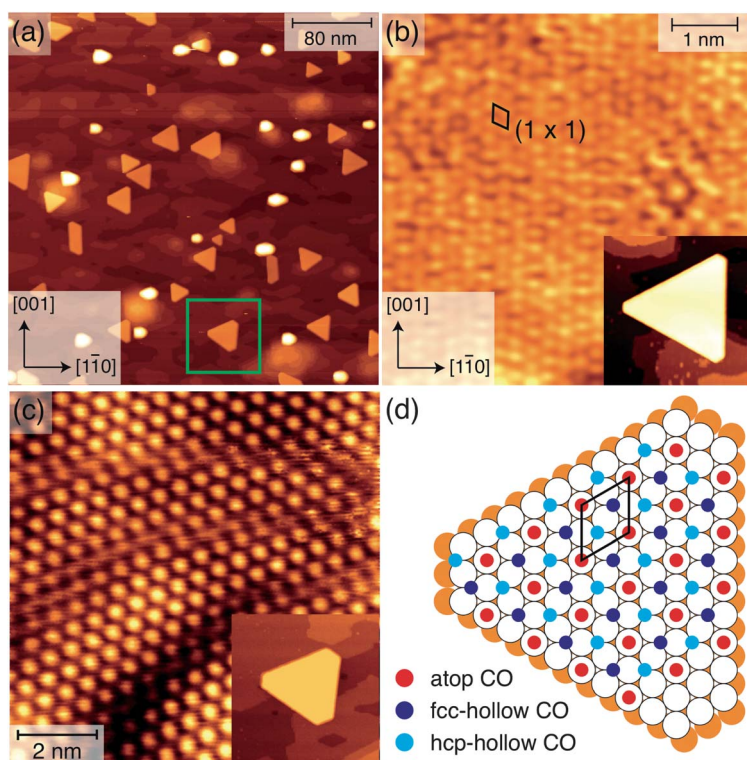


Fig. 2 (a) STM image (390×390 nm², 1.6 V, 10 pA) of Pd islands distributed on the $\text{TiO}_2(110)$ surface. The islands are pseudo-hexagonal and have mean measured heights and diameters of 2.38 ± 0.44 nm and 22.0 ± 5.2 nm, respectively. (b) Atomically-resolved STM image acquired on a Pd nanocrystal (5.5×5.5 nm², -0.3 V, 0.2 nA) with a coverage of < 0.3 ML of CO. Due to an adventitious tip change, in contrast to most images, the underlying Pd(111)-(1 \times 1) top facet was resolved. (c) Molecularly resolved STM image (9×9 nm², 1.1 V, 10 pA) recorded on top of one of the Pd islands following a saturation dose of CO at 124 K. This leads to the formation of a (2 \times 2)-3CO ordered phase giving a CO coverage of 0.75 ML. This image was taken from the island indicated with the green square in (a) and inset in (c). (d) The proposed model for (2 \times 2)-3CO, with CO occupying atop, as well as fcc- and hcp- hollow sites. All STM data were recorded at 124 K. The $\text{TiO}_2(110)$ azimuths are indicated.

To dose CO onto the surface *via* the directional doser, the STM is paused and the tip retracted by 20 nm. Fig. 2c shows a STM image of the surface following CO dosing with nominal pressure and duration of 1×10^{-7} mbar and 3 s, respectively, at a temperature of 124 K. This dose is equivalent to a nominal 0.23 L exposure. This procedure led to saturation of CO on the {111} top facet of the Pd islands. As the doser was directed towards the surface only 50 mm away, the local pressure around the sample was estimated to be 100 times higher than that measured by the ion gauge. The estimation was made based on the exposure required to form a saturated CO overlayer without directional dosing.

Zooming into the island indicated with a green square in Fig. 2a reveals the presence of an ordered CO layer as shown in Fig. 2c. The ordered structure consists of hexagonally packed bright dots with a nearest neighbour distance of 550 ± 16 pm. The principal axes of this overlayer run parallel to those of the Pd(111) top facet so that the structure has a (2×2) arrangement. According to Rose *et al.*'s STM work on the native Pd(111) single crystal surface,²⁸ the (2×2) configuration is found when the CO coverage is 0.75 ML, where a monolayer (ML) corresponds to 1.527×10^{15} molecules cm^{-2} . Each primitive unit cell contains three CO molecules, so the overlayer is described as (2×2) -3CO. In their model, one CO molecule occupies the atop site while the other two CO molecules occupy the fcc and hcp hollow sites (Fig. 2d). The overlayer in Fig. 2c is strikingly similar to that reported by Rose *et al.*²⁸ and we therefore made the same assignment.

In order to characterise under-saturated CO overlayers, we investigated the evolution of CO structures as a function of coverage by dosing small quantities of CO in a stepwise manner. Because the Pd nanocrystals can be easily contaminated by residual CO, every time after we saturated the sample with CO, we warmed the STM from the imaging temperature of 124 K up to 200 K in order to desorb physisorbed CO from the STM stage and the cryostat. After this, a freshly-prepared Pd/TiO₂(110) sample was inserted into the microscope and held at 124 K.

Following a nominal 0.01 L CO exposure, an ordered structure was formed. As shown in Fig. 3a, it consists of hexagonally-packed unit cells with a measured unit cell parameter of 470 pm. The unit cell is rotated by 30° with respect to the Pd(111)-(1 × 1) unit cell, as judged from the step-edges of the Pd island (inset of Fig. 3a). This corresponds to a $(\sqrt{3} \times \sqrt{3})R30^\circ$ configuration, a structure previously reported for the single crystal surface that has a coverage of 1/3 ML.²⁸ The model for this overlayer has CO occupying fcc-hollow sites and is shown in Fig. 3b.

With our experimental setup it was difficult to prepare a Pd/TiO₂(110) surface covered with exactly 0.5 ML. When deviating from this coverage, the CO becomes too mobile to image in STM. To circumvent this, we adopted the following approach: first we saturated the Pd/TiO₂(110) surface with CO at 150 K, then warmed it to >200 K before bringing it back to 150 K. This led to a surface with the (111) top facet of every Pd nanocrystal covered with a $c(4 \times 2)$ -2CO overlayer. On one of the Pd nanocrystals (Fig. 3c), CO molecules arrange themselves to form a zigzag pattern. Therefore, we propose that in the $c(4 \times 2)$ -2CO structure in Fig. 3c, CO molecules occupy both fcc- and hcp- hollow sites, leading to a hollow-hollow (*hh*-) $c(4 \times 2)$ -2CO (Fig. 3d). This structure is reminiscent of similar images observed by Rose *et al.*²⁸ for CO adsorbed on the native Pd(111) surface.

Fig. 3c also shows a facet edge on the right-hand side. Note that the structure deviates from that of the (111) top facet: the protrusions along the facet edge appear with varying brightness in STM. In the *hh*- $c(4 \times 2)$ -2CO structure proposed for the (111) top facet, CO at both fcc- and hcp- hollow sites appear with equal brightness. As such, we believe that those protrusions arise from the CO adsorbing at the sites on the {111} side facet, or less likely, along the edge of the top facet (which comprises only atop sites and bridge sites). Judging from their positions and relative brightness, we attribute those protrusions to CO that occupy different adsorption sites on the {111} side facet. The brighter protrusions correspond to CO that occupy hcp-hollow sites, and the dimmer protrusions to CO that occupy fcc-hollow sites

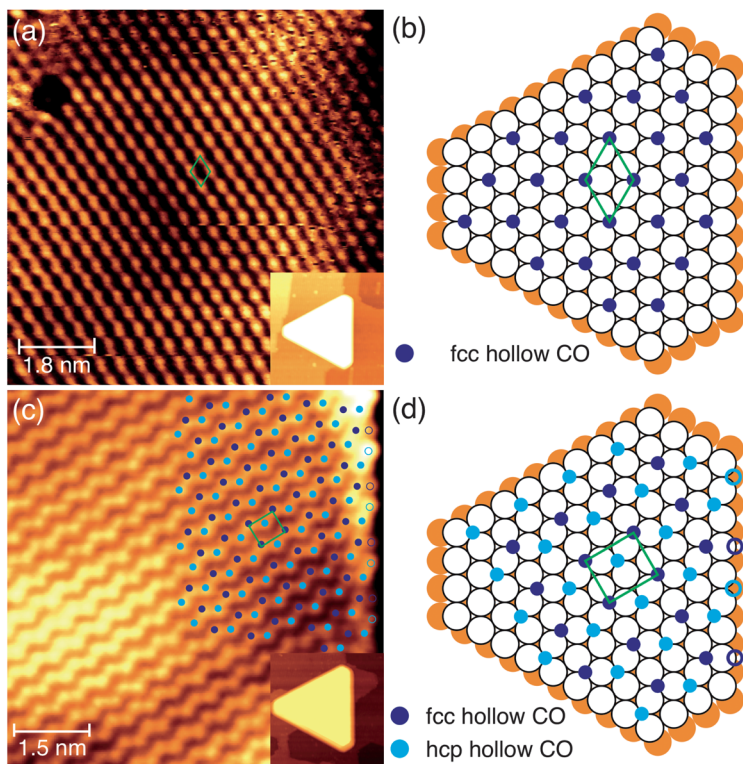


Fig. 3 (a) Molecularly resolved STM image ($9 \times 9 \text{ nm}^2$, 0.9 V, 0.05 nA) recorded on a Pd nanocrystal (width = 22.3 nm, height = 3.0 nm) at 124 K. The (111) top-facet of the Pd nanocrystal was covered with 0.33 ML of CO. (b) A ball model showing how CO bonds to the (111) top facet of a nanocrystal in the proposed $(\sqrt{3} \times \sqrt{3})R30^\circ\text{-1CO}$ structure. (c) Molecularly resolved STM image ($7.6 \times 7.6 \text{ nm}^2$, 0.5 V, 0.1 nA) recorded on a Pd nanocrystal (width = 29.1 nm, height = 2.7 nm) at 150 K. Its (111) top facet was covered with 0.5 ML of CO, prepared with non-directional dosing method (see text). (d) A ball model of $h\bar{h}\text{-c}(4 \times 2)\text{-2CO}$ ordered structure. CO occupying the fcc- and hcp- hollow sites on the {111} side facet are indicated with open circles. The $\text{TiO}_2(110)$ azimuths are shown in Fig. 2.

(marked with open circles in Fig. 3). This assignment is based on the higher vertical positions of the hcp-hollow sites on the {111} side facets compared with the fcc-hollow sites. This bonding of CO on the {111} side facet is also illustrated in Fig. 3d.

We can compare the overlayers observed in STM with their adsorption energies computed using the VASP code. The latter are shown in Table 1 where it can be seen that the lowest energy adsorption sites are in line with those calculated in the earlier work.¹⁵ In other words, at 0.33 ML, fcc hollow sites are occupied, while at 0.5 ML both fcc and hcp hollow sites are occupied. At 0.75 ML atop sites along with fcc and hcp hollow sites are filled. The inclusion of vdW contributions increases the adsorption energies (up to 0.3 eV molecule⁻¹ for the 0.75 ML coverage) but does not modify the relative stability of the different sites for a given coverage.

O₂ adsorption on Pd nanocrystals

We also investigated O₂ adsorption on the Pd nanocrystals with STM. Following a nominal O₂ exposure of 0.005 L on the Pd/TiO₂(110) surface by directional dosing at 190 K, an oxygen-induced ordered structure was formed on the (111) top facet of the Pd nanocrystals, as shown in Fig. 4a. The ordered structure consists of hexagonally

Table 1 PBE + vdW calculated adsorption energies E_{ads} (eV) and adsorption energies per molecule $E_{\text{ads}} \text{ mol}^{-1}$ (eV) for the chemisorption of CO on Pd(111), at coverages 0.33 ML [$(\sqrt{3} \times \sqrt{3})\text{R}30^\circ\text{-1CO}$], 0.5 ML [$\text{c}(4 \times 2)\text{-2CO}$] and 0.75 ML [$(2 \times 2)\text{-3CO}$]

Structure	$(\sqrt{3} \times \sqrt{3})\text{R}30^\circ\text{-1CO}$				$\text{c}(4 \times 2)\text{-2CO}$		$(2 \times 2)\text{-3CO}$	
Coverage	$\theta = 0.33 \text{ ML}$				$\theta = 0.50 \text{ ML}$		$\theta = 0.75 \text{ ML}$	
Sites	atop	bridge	hollow fcc	hollow hcp	bridge-bridge	fcc + hcp	atop + bridge-bridge	atop + fcc + hcp
E_{ads} (eV)	-1.5860	-2.0023	-2.1958	-2.1594	-4.1834	-4.2923	-3.7242	-5.3351
$E_{\text{ads}} \text{ mol}^{-1}$ (eV)	-1.5860	-2.0023	-2.1958	-2.1594	-2.0917	-2.1462	-1.2414	-1.7784

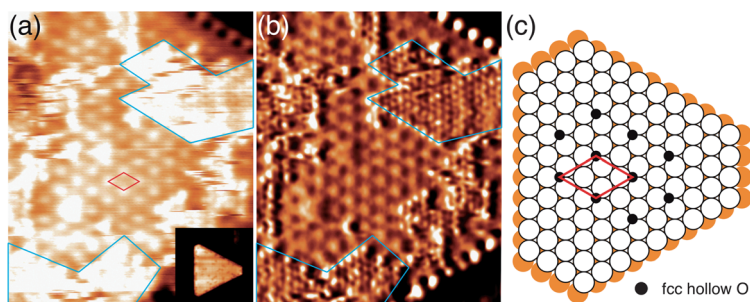


Fig. 4 (a) Atomically resolved STM image ($8.0 \times 9.3 \text{ nm}^2$, 0.45 V, 0.15 nA) recorded on a Pd nanocrystal (diameter = 15.0 nm, height = 1.9 nm) at 190 K. Its (111) top facet was partially covered with $< 0.25 \text{ ML}$ of atomic oxygen, leading to the formation of a $\text{p}(2 \times 2)\text{-O}$ structure. Edge structures are also observed on the top- and bottom-right of the image. (b) The corresponding current map of (a) illustrates that the unresolved areas (highlighted in blue) in (a) are the (111) top-facet regions not covered with atomic O, as the (111)- (1×1) unit cells are resolved. (c) Ball model of the $\text{p}(2 \times 2)\text{-O}$ ordered phase, in which atomic O is proposed to adsorb at the fcc-hollow sites.

packed bright dots with a nearest neighbour distance of $550 \pm 20 \text{ pm}$. The principal axes of this overlayer run parallel to those of the Pd(111) top facet so that the structure has a (2×2) arrangement. As O_2 thermally dissociates to form atomic-O pairs on Pd(111) at 160 K,²⁹ we believe that the (2×2) ordered structure on the {111} top facet consists of atomic oxygen, leading to $\text{p}(2 \times 2)\text{-O}$. In the ball model in Fig. 4c, we propose that in the $\text{p}(2 \times 2)\text{-O}$ structure, oxygen atoms adsorb at the fcc-hollow sites. These sites have been shown to be most favoured on the (111) surface of Pd single crystals.^{29,30} Note that some areas (highlighted in blue) in the STM topography image are not well resolved (Fig. 4a). However, those areas are resolved in the current map recorded simultaneously (Fig. 4b). In the current map, the areas which are unresolved in Fig. 4a can be seen to consist of hexagonally packed bright dots with a nearest neighbour distance of $271 \pm 20 \text{ pm}$, consistent with the Pd lattice constant of 2.75 Å. From this, we conclude that those areas are parts of the top facet not covered with atomic oxygen. Apart from the top-facet region, we also observed some edge structures on the oxygen-covered Pd nanocrystals, as shown in the top- and bottom-right of the images in Fig. 4a and 4b. Those edge structures look very similar to one of those reported in Højrup-Hansen *et al.*'s work.⁸ As yet we do not have a model for this observed edge structure.

4 Summary

We have prepared a model catalytic system by forming Pd nanocrystals on rutile TiO₂(110). Those nanocrystals, with average diameter of ~22 nm and height of ~2 nm, consist of (111) top facets with {111} and {100} side facets. The top facets can be imaged with atomic resolution, confirming the Pd(111)-(1 × 1) long range order expected and also demonstrating that the nanocrystals are not encapsulated. By varying the CO exposure, a rich variety of CO overlayers were formed on the (111) top facets with coverages ranging from 1/3 ML to the saturated 3/4 ML (2 × 2)-3CO overlayer. Importantly, some of these overlayers were under-saturated and are therefore likely to be more reactive than the saturated (2 × 2)-3CO layer. DFT calculations of adsorption energies indicate that for all the structures observed, fcc-hollow sites are occupied. Above 0.33 ML, first hcp hollow sites are occupied and then additionally the atop site at 0.75 ML. By dosing a small amount of O₂ on Pd/TiO₂(110) at 190 K, we observed the formation of the p(2 × 2)-O ordered structure as well as oxygen-induced edge structures on the island edges. Island edges and island–oxide interface regions have long been posited as active sites for catalysis and our model system offers the opportunity to study any such effect directly with STM. This work shows that adsorbate overlayers can be the same on nanoparticles as those observed on metal single crystal surfaces, even below saturation coverage. However, in a future publication we will present data that evidences significant differences in behaviour.

Acknowledgements

This work was supported by EPSRC (UK), COST1104 and European Research Council Advanced Grant ENERGYSURF. RP acknowledges the support of the Spanish Projects MAT2011-023627 (MINECO), PR2011-0402 (MEC) and Fundación CajaMadrid.

References

- 1 V. P. Zhdanov and B. Kasemo, *Surf. Sci. Rep.*, 2000, **39**, 25–104.
- 2 W. C. Conner and J. L. Falconer, *Chem. Rev.*, 1995, **95**, 759–788.
- 3 S. J. Tauster, *Acc. Chem. Res.*, 1987, **20**, 389–394.
- 4 Z. Chang and G. Thornton, *Surf. Sci.*, 2000, **459**, 303–309.
- 5 M. Bowker, P. Stone, R. A. Bennett and N. Perkins, *Surf. Sci.*, 2002, **497**, 155–165.
- 6 O. Dulub, W. Hebenstreit and U. Diebold, *Phys. Rev. Lett.*, 2000, **84**, 3646–3649.
- 7 R. A. Bennett, C. L. Pang, N. Perkins, R. D. Smith, P. Morrall, R. I. Kvon and M. Bowker, *J. Phys. Chem. B*, 2002, **106**, 4688–4696.
- 8 K. Højrup Hansen, Ž. Šljivančanin, E. Laegsgaard, F. Besenbacher and I. Stensgaard, *Surf. Sci.*, 2002, **505**, 25–38.
- 9 W. Gao, J. Chen, X. Guan, R. Jin, F. Zhang and N. Guan, *Catal. Today*, 2004, **93–95**, 333–339.
- 10 W. Kim, *J. Catal.*, 2004, **226**, 226–229.
- 11 H. Imagawa, T. Tanaka, N. Takahashi, S. Matsunaga, A. Suda and H. Shinjoh, *J. Catal.*, 2007, **251**, 315–320.
- 12 H. Ohtani, M. A. V. Hove and G. A. Somorjai, *Surf. Sci.*, 1987, **187**, 372–386.
- 13 S. Surnev, M. Sock, M. G. Ramsey, F. P. Netzer, M. Wiklund, M. Borg and J. N. Andersen, *Surf. Sci.*, 2000, **470**, 171–185.
- 14 M. K. Rose, T. Mitsui, J. Dunphy, A. Borg, D. F. Ogletree, M. B. Salmeron and P. Sautet, *Surf. Sci.*, 2002, **512**, 48–60.
- 15 D. Loffreda, D. Simon and P. Sautet, *Surf. Sci.*, 1999, **425**, 68–80.
- 16 M. Dion, H. Rydberg, E. Schröder, D. C. Langreth and B. I. Lundqvist, *Phys. Rev. Lett.*, 2004, **92**, 246401; M. Dion, H. Rydberg, E. Schröder, D. C. Langreth and B. I. Lundqvist, *Phys. Rev. Lett.*, 2005, **95**, 109902.
- 17 D. C. Langreth, M. Dion, H. Rydberg, E. Schröder, P. Hyldgaard and B. I. Lundqvist, *Int. J. Quantum Chem.*, 2005, **101**, 599–610.
- 18 P. Lazić, M. Alaci, N. Atodiresci, V. Caciuc, R. Brako and S. Blügel, *Phys. Rev. B*, 2010, **81**, 045401.

-
- 19 J. Klimeš, D. R. Bowler and A. Michaelides, *J. Phys.: Condens. Matter*, 2010, **22**, 022201.
 - 20 J. Klimeš, D. Bowler and A. Michaelides, *Phys. Rev. B*, 2011, **83**, 195131.
 - 21 R. Nyholm, J. N. Andersen, U. Johansson, B. N. Jensen and I. Lindau, *Nucl. Instrum. Methods Phys. Res., Sect. A*, 2001, **467–468**, 520–524.
 - 22 G. Kresse and J. Furthmüller, *Comput. Mater. Sci.*, 1996, **6**, 15–50.
 - 23 G. Kresse, *Phys. Rev. B*, 1996, **54**, 11169–11186.
 - 24 G. Román-Pérez and J. Soler, *Phys. Rev. Lett.*, 2009, **103**, 096102.
 - 25 M. Bowker, P. Stone, P. Morrall, R. Smith, R. A. Bennett, N. Perkins, R. Kvon, C. L. Pang, E. Fourre and M. Hall, *J. Catal.*, 2005, **234**, 172–181.
 - 26 J. Stohr and D. A. Outka, *Phys. Rev. B*, 1987, **36**, 7891–7905.
 - 27 J.-H. Fischer-Wolfarth, J. Farmer, J. Flores-Camacho, A. Genest, I. Yudanov, N. Rösch, C. Campbell, S. Schauer mann, and H.-J. Freund, *Phys. Rev. B*, 2010, **81**, 241416.
 - 28 M. K. Rose, T. Mitsui, J. Dunphy, A. Borg, D. F. Ogletree, M. B. Salmeron and P. Sautet, *Surf. Sci.*, 2002, **512**, 259–266.
 - 29 M. K. Rose, A. Borg, J. C. Dunphy, T. Mitsui, D. F. Ogletree and M. B. Salmeron, *Surf. Sci.*, 2004, **561**, 69–78.
 - 30 J. Blanco, C. González, P. Jelinek, J. Ortega, F. Flores, R. Pérez, M. K. Rose, M. B. Salmeron, J. Méndez, J. Wintterlin and G. Ertl, *Phys. Rev. B*, 2005, **71**, 113402.